A VNS algorithm for the design of supplementary damping controllers for small-signal stability analysis

Elenilson de Vargas Fortes [a],[*],[1], Leonardo H. Macedo [b], Percival Bueno de Araujo [b], Rubén Romero [b]

[a] Goiás Federal Institute of Education, Science and Technology, Rua Maria Vieira Cunha, 775, Residencial Flamboyant, 75804-714 Jataí, GO, Brazil
[b] São Paulo State University, Avenida Brasil 56, Centro, PO Box 31, 15385-000 Ilha Solteira, SP, Brazil

ARTICLE INFO

ABSTRACT

This paper presents a variable neighborhood search (VNS) optimization algorithm for the design of the parameters of supplementary damping controllers: power system stabilizers (PSS) and the interline power flow controller–power oscillation damping (IPFC–POD) set. The objective is to insert damping to local and inter-area oscillation modes in multimachine power systems. The electric power system dynamics is represented by the current sensitivity model. Simulations were carried out using three systems: a test system known as Two-Area Symmetrical and two real systems, the New England and the Reduced Southern Brazilian. The VNS method was compared with a multi-start algorithm in terms of performance, showing better convergence rates. The proposal was also able to obtain solutions with high damping levels, that showed to be robust when changes on the operating point of the power system were considered. Finally, it has been verified that the PSS controllers were effective for damping the local mode oscillations, while the IPFC–POD set operated mainly damping the inter-area modes.

© 2017 Elsevier Ltd. All rights reserved.

1. Introduction

Stability studies can be divided into two distinct branches: transient and dynamic stability. Transient stability deals with the first oscillations that occur in the system after a large disturbance, such as short circuits in the transmission network or loss of a generating unit. On the other hand, the dynamic stability, or small-signal stability, the focus of this work, is limited to the restoration of the steady state operation of the system after the occurrence of small disturbances that are often caused by small variations of loads [1].

In the literature, the problems of electromechanical oscillations are treated in different ways and can be of a local or global nature. Local problems involve a small part of the power system, and they are usually associated with the rotor angle oscillations of a generating unit and the rest of the system or another generating unit within its area. These oscillations are defined as local mode oscillations, and their frequencies of occurrence are within the range of 0.8–2.0 Hz [2].

The global problems are caused by interactions among a large number of generating units and basically involve a group of generators located in an area oscillating coherently against another group of generators, located on adjacent areas. These oscillations are referred to as inter-area modes, with oscillation frequencies in the range of 0.2–0.7 Hz, occurring particularly when the systems are connected by relatively weak lines, i.e., lines with much lower capacity than the capacity of the systems that they interconnect [2,3].

To insert damping to these oscillations present in the electric power system, control strategies should be applied. These strategies are based on two types of controllers, known in the literature as the power system stabilizer (PSS) [2,4] and power oscillation damping (POD) [5]. The PSSs are added to the control loop of the automatic voltage regulator (AVR) of synchronous generators and

Nomenclature

$\Delta\omega_k$	variation in the angular velocity of the rotor of generator k
ΔE_k^{fd}	field voltage of generator k
ΔP_{km}	deviation in the active power of branch km
ΔV_k	magnitude of the terminal voltage of the generator k
$\Delta V_{1_k}, \Delta V_{2_k}$	intermediary signals of the PSS dynamic model
ΔV_j^p	output modulated by the POD
ΔV_k^{ref}	reference voltage of the AVR at generator k
ΔV_1^{sup}	output signal from the PSS
ΔV_2^{sup}	output signal from the POD
$\Delta Y_1, \Delta Y_2, \Delta Y_3$	intermediary signals of the POD's dynamic model
ΔX^{ref}	input signal of the POD
λ_i	dominant eigenvalue i
σ_i	real part of λ_i
ω_i	imaginary part of λ_i
ω_{n_i}	natural undamped frequency related to eigenvalue i
θ_i	voltage angle at bus i
ξ_i	damping of eigenvalue i
$\underline{\xi_i}$	minimum damping for eigenvalue i
$\overline{b}_{ij}, r_{ij}, x_{ij}$	susceptance, resistance, and reactance of branch ij
b_{ij}^{sh}	shunt susceptance of branch ij
D_k	damping torque coefficient of the electromechanical loop of generator k
H_k	inertia constant of generator k
$\mathbf{I}_{ij}$	current phasor on branch ij
$I_i^{inj,r}, I_i^{inj,m}$	real and imaginary components of the current injection at bus i by the IPFC
I_{ij}^r, I_{ij}^m	real and imaginary components of $\mathbf{I}_{ij}$
I_i^r, I_i^m	real and imaginary components of the current injection at bus i
$K_1^{pi}, K_2^{pi}, K_3^{pi}$	gains of the PI controllers
K^{pod}	gain of the POD
K^{pss}	gain of the PSS
K_k^r	gain of the AVR of generator k
P_{ki}, Q_{ki}	active and reactive power flows on branch ki
P_i, Q_i	active and reactive power injections at bus i
P_{ij}^c, Q_{ij}^c	active and reactive controlled power flows on branch ij
P_j^g, Q_j^g	active and reactive power generations at bus j
P_i^{inj}	active power injected at bus i by the IPFC
P_j^l, Q_j^l	active and reactive power demands at bus j
$P_{ij}^{ref}, Q_{ij}^{ref}$	active and reactive reference power flows on branch ij
$T'_{d_{0k}}$	transient direct axis open-circuit time constant of generator k
$T_1^{pi}, T_2^{pi}, T_3^{pi}$	time constants of the PI controllers
T_ω^{pod}	time constant of the washout block of the POD model
T_ω^{pss}	time constant of the washout block of the PSS model
$T_1^{pss}, T_2^{pss}, T_3^{pss}, T_4^{pss}$	time constants of the PSS
T_m^{ipfc}	inherent delay of the control system of the IPFC
$T_1^{pod}, T_2^{pod}, T_3^{pod}, T_4^{pod}$	time constants of the IPFC–POD set
T_k^r	time constant of the AVR of generator k
V_i	voltage magnitude at bus i
$\mathbf{V}'_k$	complex voltage on the fictitious bus k'
V_n^q, V_n^p	direct and quadrature components of the series voltage source at bus n
$\dot{V}_n^p, \dot{V}_n^q$	time derivatives of V_n^p and V_n^q
$\mathbf{V}_n^{pq}$	series synchronous controllable voltage source at bus n
V^{sup}	output signal of the POD controller
X_1, X_2, X_3	input signals of the PI controllers
$\dot{X}_1, \dot{X}_2, \dot{X}_3$	time derivatives of X_1, X_2, and X_3
x_{d_k}, x_{q_k}	direct and quadrature axis synchronous reactances of generator k
x'_{d_k}	direct axis transient reactance of generator k

operate inserting damping to local mode oscillations, if their control parameters (time constants and gains) are adjusted correctly [3,6]. The POD device can be used to increase the stability limits related to inter-area modes, if the device's control parameters (time constants and gain) are properly adjusted. The POD must also operate jointly with flexible AC transmission system (FACTS) devices. In this work, the FACTS interline power flow controller (IPFC) is considered [7].

Two types of analyzes will be performed: the static and the dynamic. Regarding the static analysis, the IPFC device is used to control, simultaneously or selectively, the power flow in certain transmission lines. Regarding the dynamic analysis, the structure of the IPFC's control system is modeled using proportional-integral (PI) controllers [3,6]. This model will be used to analyze the influence of the IPFC on small-signal stability in the electric power system.

To provide damping to unstable or low-damped modes of the electric power system and, thereby, increase its stability limits, a coordinated project of the supplementary controllers, PSS and IPFC–POD, is implemented. Among the existing methods in the literature, there are the classical methods and optimization techniques. The decentralized modal control (DMC), residue, and Nyquist's stability criterion are classified as classical methods [6,8–10].

The optimization algorithms are an alternative to the classical techniques for the design of these controllers. Since this design problem is nonlinear and has both algebraic and differential equations in the formulation, metaheuristics are suitable methods to be applied. In this context, the bacterial foraging optimization (BFO) algorithm is used in [11] to design the PSSs and in [12] to perform the coordinated design of PSSs and static var compensator (SVC) to improve the stability of the system. In [13], a particle swarm optimization (PSO) algorithm is presented to both allocate and set the parameters of SVCs and thyristor controlled series compensators (TCSC) to damp small-signal oscillations in multimachine power systems. Ref. [14] proposes a PSO algorithm to allocate and tune the parameters of PSSs and TCSCs to mitigate inter-area oscillations. Ref. [15] proposes a PSO algorithm for the coordinated design of PSS and TCSC in multimachine power systems. The genetic algorithm (GA) is used in [16] to perform the design of PSSs and unified power flow controller (UPFC) and in [17] to design PSSs and static synchronous series compensators (SSSC). In [18], the modified fruit fly optimization algorithm (MFOA) is used to perform the design of PSSs and SVC to improve small-signal stability in power systems with wind energy generation. The seeker optimization algorithm (SOA) is presented in [19] to coordinate PSSs and SSSC. A cuckoo search algorithm is proposed in [20] to design PSSs considering various operation conditions and disturbances in the power system. Ref. [21] presents a simulated annealing (SA) algorithm for the tuning of PSSs and the IPFC–POD.

Also, hybrid versions of optimization algorithms can be found, such as the hybrid bacteria foraging optimization–particle swarm optimization algorithm (hBFOA–PSO), that was used in [22] to perform the design of PSSs and SSSC, and in [23] for the design of TCSC. Finally, the hybrid particle swarm optimization–gravitational search algorithm (hPSO–GSA) was presented in [24] for the coordinated design of PSSs and SSSC.

In this study, a metaheuristic known as variable neighborhood search (VNS) [25] is used to perform the design of the parameters of the supplementary damping controllers, PSS and IPFC–POD. The VNS algorithm has shown excellent results in the field of Operations Research, but has not been explored in optimization problems of Electrical Engineering. The main advantage of the proposed technique is that it does not require defining and tuning parameters, such as the size of the population, mutation rate, etc., that are required, for example, in GAs. Most of the existing methods presented in the literature require tuning the algorithm to each instance of the problem, whereas the proposed VNS method can be applied, as it will be shown, to solve various instances of the problem without any modification. The proposed method has a local search strategy based on a cyclic coordinate method that uses a Fibonacci method to perform a line search. To validate the proposed technique, the performance of the VNS algorithm was compared to a multi-start algorithm [26]. Three test systems are considered: a small system known as Two-Area Symmetrical [1], and two real medium-sized systems, the New England [3] and the Reduced Southern Brazilian.

To represent the electric power system dynamics, the current sensitivity model (CSM) [3] was used, whose main concept is based on Kirchhoff's current law, which must be satisfied in all dynamic processes in the electric power system.

In this context, the main contributions of this work are as follows: (1) to implement computationally a VNS algorithm to perform the design of the PSS and IPFC–POD controllers; (2) to validate the VNS algorithm as an optimization technique for adjusting the parameters of the PSS and IPFC–POD controllers; and (3) to analyze the efficiency of the PSS and IPFC–POD controllers when the goal is to insert damping to local and inter-area oscillation modes.

The remaining of the paper is organized as follows: Section 2 presents the model for the operation and control of the IPFC, while Section 3 shows the dynamic models for the PSS and POD controllers. Section 4 introduces the proposed VNS algorithm for the design of the PSS and POD controllers. Since the algorithms are presented in a general way in Section 4, Section 5 presents the details of the implementation of the optimization technique for the considered problem, based on the modeling presented in Sections 2 and 3. Section 6 presents the results of the work, including both static and dynamic analysis for the three systems, analysis of the performance of the proposed VNS algorithm, and a discussion about the results. Finally, Section 7 presents the conclusions and future work.

2. Interline power flow controller

The IPFC device can control power flows across lines, reducing overloads and compensating for voltage magnitude drops [7]. In Fig. 1, an equivalent circuit for the IPFC, with two voltage source converters (VSC), connected to the AC network via coupling transformers, is shown.
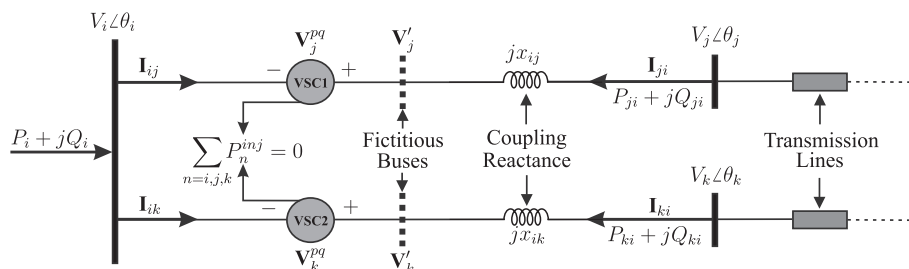
In Fig. 1, the IPFC is represented by two synchronous voltage sources injecting a series controllable voltage $\mathbf{V}_n^{pq}$ ($n = j, k$). Each voltage source is in series with its respective reactance (x_{in}, $n = j, k$) of the coupling transformer. The quantities P_i and Q_i are injections of active and reactive power in bus i. In addition, $P_{ji}, P_{ki}, Q_{ji}, Q_{ki}$, and $\mathbf{I}_{ij}, \mathbf{I}_{ik}, \mathbf{I}_{ji}$, and $\mathbf{I}_{ki}$ are, respectively, the active and reactive power flows and current phasors circulating on the lines between buses j and k. The variables $\mathbf{V}_j'$ and $\mathbf{V}_k'$ are the voltages on the fictitious buses j' and k' and are included in the system for the deduction of the current injection model for the IPFC. Assuming that the active losses are zero, it follows that $\sum_{n=i,j,k} P_n^{inj} = 0$, i.e., the active power provided by one of the converters (VSC1) will always be equal to the active power demanded by the other (VSC2). This restriction is known as the active power invariance of the IPFC [27].

2.1. Current injection model for the IPFC

Eqs. (1)–(4) represent the current injection equations for the IPFC, presented in [3,6], that can be obtained based on Fig. 1.

$$I_i^r = -V_i \sin \theta_i (b_{ij} + b_{ik}) + b_{ij} V_j \cos \theta_j + b_{ik} V_k \sin \theta_k$$
$$- \underbrace{\sum_{n=j,k} b_{in} (V_n^p \cos \theta_i + V_n^q \sin \theta_i)}_{I_i^{inj,r}} \quad (1)$$

$$I_i^m = V_i \cos \theta_i (b_{ij} + b_{ik}) - \sum_{n=j,k} b_{in} V_n \cos \theta_n$$
$$+ \underbrace{\sum_{n=j,k} b_{in} (V_n^q \cos \theta_i - V_n^p \sin \theta_i)}_{I_i^{inj,m}} \quad (2)$$

$$I_{ni}^r = b_{in} (V_i \sin \theta_i - V_n \sin \theta_n) + \underbrace{b_{in} (V_n^p \cos \theta_i + V_n^q \sin \theta_i)}_{I_n^{inj,r}} \quad (3)$$

$$I_{ni}^m = b_{in} (V_n \cos \theta_n - V_i \cos \theta_i) + \underbrace{b_{in} (V_n^p \sin \theta_i - V_n^q \cos \theta_i)}_{I_n^{inj,m}} \quad (4)$$

In (1)–(4), $b_{in} = -\frac{1}{x_{in}}$ for $n = j, k$. Additionally, I_i^r and I_i^m in (1) and (2) are the real and imaginary components of the current injection at bus i. Variables $I_n^{inj,r}$ and $I_n^{inj,m}$ in (3) and (4) are the current injections in bus n ($n = j, k$) by the IPFC, the real and imaginary axis components, respectively.

2.2. Structure of the IPFC control system

With the current injection model for the IPFC presented, the next step is to derive a structure that represents the device's control system. PI controllers are used in the structure of the IPFC control system. Based on the fact that the quadrature components of the series voltage sources produce strong impact on active power flows and the in-phase components have significant effects on the reactive power flows, each controller shown in Fig. 2 is related

Fig. 1. Equivalent circuit of an IPFC with two series voltage sources.

to a variable of the controllable sources (V_j^p, V_j^q, and V_k^p), except the variable V_k^q, which is related to the equation of the invariance of the active power of the IPFC. The objective is to properly modulate, reducing the difference between the reference values and the measured values in the transmission lines, the active and reactive power flows that the IPFC device can control [3,6,28].

In the structure shown in Fig. 2, the controlled flows are P_{ij}^c, P_{ik}^c, and Q_{ij}^c, while the reference ones are P_{ij}^{ref}, Q_{ij}^{ref}, and Q_{ik}^{ref}. The time constant T_m^{ipfc} is the inherent delay of the control system and is in the range of 1–10 ms [2]. The parameters of the PI controllers are the gains (K_1^{pi}, K_2^{pi}, and K_3^{pi}) and the time constants (T_1^{pi}, T_2^{pi}, and T_3^{pi}). The signal V^{sup} comes from the POD controller that, in this work, will be used to modulate the variable V_j^p and, thus, provide damping to the oscillations of the electric power system. The signals X_1, X_2, and X_3 are input signals that are specified.

The dynamic behavior of the control structure shown in Fig. 2 for the IPFC device is given by (5)–(10), obtained by inspection.

$$\dot{V}_j^p = \frac{K_1^{pi}}{T_m^{ipfc}}\left(P_{ij}^{ref} - P_{ij}^c\right) + \frac{1}{T_m^{ipfc}}\left(X_1 + V^{sup} - V_j^p\right) \tag{5}$$

$$\dot{X}_1 = \frac{1}{T_1^{pi}}\left(P_{ij}^{ref} - P_{ij}^c\right) \tag{6}$$

$$\dot{V}_j^q = \frac{K_2^{pi}}{T_m^{ipfc}}\left(Q_{ij}^{ref} - Q_{ij}^c\right) + \frac{1}{T_m^{ipfc}}\left(X_2 - V_j^q\right) \tag{7}$$

$$\dot{X}_2 = \frac{1}{T_2^{pi}}\left(Q_{ij}^{ref} - Q_{ij}^c\right) \tag{8}$$

$$\dot{V}_k^p = \frac{K_3^{pi}}{T_m^{ipfc}}\left(P_{ik}^{ref} - P_{ik}^c\right) + \frac{1}{T_m^{ipfc}}\left(X_3 - V_k^p\right) \tag{9}$$

$$\dot{X}_3 = \frac{1}{T_3^{pi}}\left(P_{ik}^{ref} - P_{ik}^c\right) \tag{10}$$

3. Supplementary damping controllers PSS and POD

This section presents the models of the PSS and IPFC–POD controllers used in this study. As shown in Fig. 3, the structures considered for both controllers are identical. They are represented by a gain (K^{pss} for the PSS and K^{pod} for the POD), a washout block (with time constant T_ω^{pss} for the PSS and T_ω^{pod} for the POD), and two phase delay blocks (with time constants $T_1^{pss}, T_2^{pss}, T_3^{pss}$, and T_4^{pss} for the PSS, and $T_1^{pod}, T_2^{pod}, T_3^{pod}$, and T_4^{pod} for the POD). However, although they have the same structures, the operation mode and the input and output signals of each controller are distinct. The PSSs are coupled to the control loop of synchronous generators, whereas the POD is inserted in the control loop of FACTS devices (in this work, the IPFC).

Note that the input signal selected for the PSS is $\Delta\omega_k$ (variations in the angular velocity of the rotor of generator k), while for the POD, the adopted signal is ΔP_{km} (deviations of the active power flow on the transmission line adjacent the IPFC–POD installation). The output of the PSS (ΔV_1^{sup}) is applied to the generator's voltage control loop, while the output of the POD (ΔV_2^{sup}) is added to the control loop of the IPFC device to modulate ΔV_j^p.
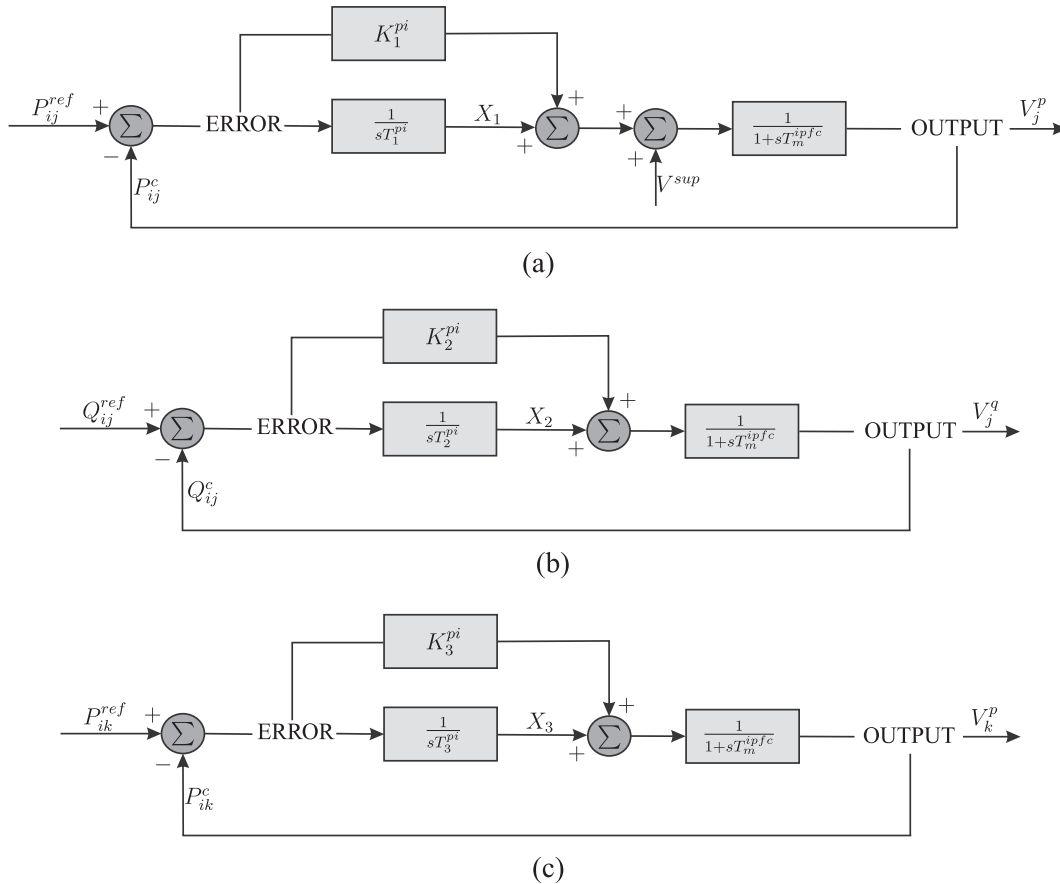

(a)

(b)

(c)

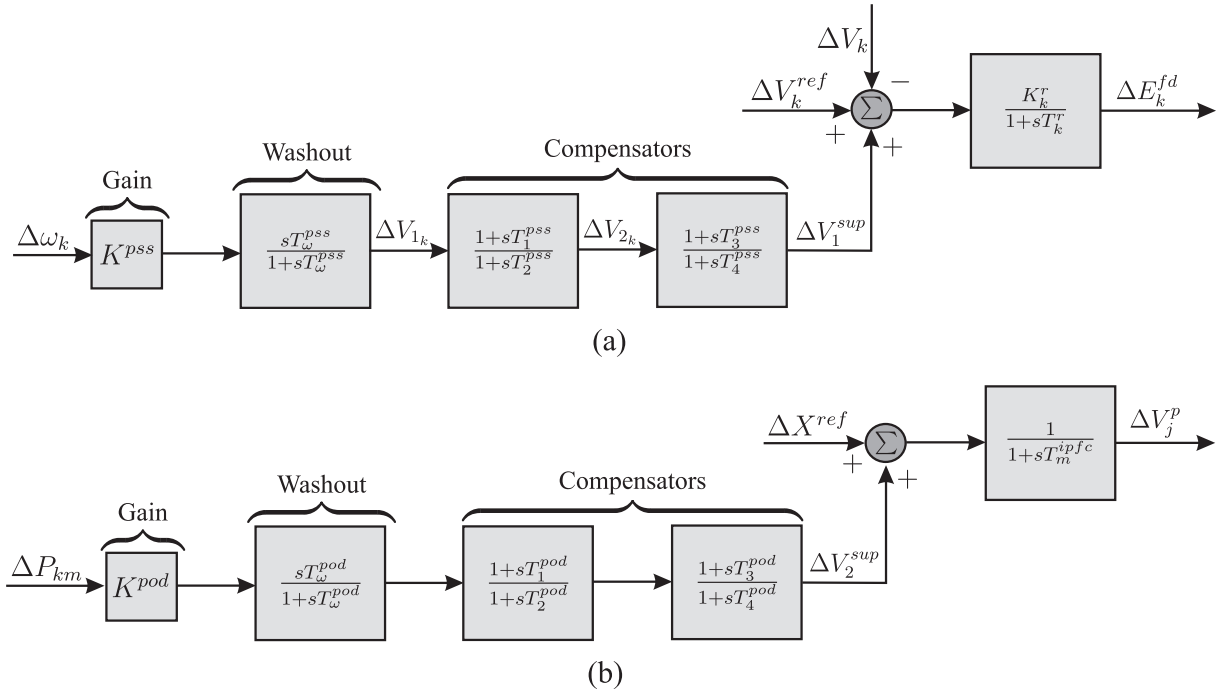**Fig. 2.** Structure of the IPFC control system.

Fig. 3. Dynamic models of the (a) PSS controller, and (b) IPFC–POD controller.

In Fig. 3(a), the AVR is represented by a gain K_k^r and a constant time T_k^r. The generator's field voltage is ΔE_k^{fd}, the magnitude of the terminal voltage is ΔV_k and the reference voltage is ΔV_k^{ref}. In Fig. 3 (b), ΔX^{ref} is the input signal and T_m^{ipfc} is the time constant, both of them specified.

By analyzing the block diagrams shown in Fig. 3, the equations that define the dynamic behavior of the PSS controllers are shown in (11)–(14), while the dynamic operation of the POD controller is described by (15)–(18).

$$\Delta \dot{V}_{1_k} = \Delta \dot{\omega}_k K^{pss} - \frac{1}{T_\omega^{pss}} \Delta V_{1_k} \tag{11}$$

$$\Delta \dot{V}_{2_k} = \frac{1}{T_2^{pss}} \Delta V_{1_k} + \frac{T_1^{pss}}{T_2^{pss}} \Delta \dot{V}_{1_k} - \frac{1}{T_2^{pss}} \Delta V_{2_k} \tag{12}$$

$$\Delta \dot{V}_1^{sup} = \frac{1}{T_4^{pss}} \Delta V_{2_k} + \frac{T_3^{pss}}{T_4^{pss}} \Delta \dot{V}_{2_k} - \frac{1}{T_4^{pss}} \Delta V_1^{sup} \tag{13}$$

$$\Delta \dot{E}_k^{fd} = \frac{K_k^r}{T_k^r} \left(\Delta V_1^{sup} + \Delta V_k^{ref} - \Delta V_k \right) - \frac{1}{T_k^r} \Delta E_k^{fd} \tag{14}$$

$$\Delta \dot{Y}_1 = \frac{1}{T_\omega^{pod}} \left(K^{pod} \Delta P_{km} - \Delta Y_1 \right) \tag{15}$$

$$\Delta \dot{Y}_2 = \frac{1}{T_2^{pod}} \left[\left(1 - \frac{T_1^{pod}}{T_2^{pod}} \right) \left(K^{pod} \Delta P_{km} - \Delta Y_1 \right) - \Delta Y_2 \right] \tag{16}$$

$$\Delta \dot{Y}_3 = \frac{1}{T_4^{pod}} \left\{ \left[\Delta Y_2 + \frac{T_1^{pod}}{T_2^{pod}} \left(K^{pod} \Delta P_{km} - \Delta Y_1 \right) \right] \left(1 - \frac{T_3^{pod}}{T_4^{pod}} \right) - \Delta Y_3 \right\} \tag{17}$$

$$\Delta \dot{V}_j^p = \frac{K_1}{T_\omega^{pod}} \left(\Delta P_j^{ref} - \Delta P_j^c \right) + \frac{1}{T_\omega^{pod}} \left(\Delta X_1 + \Delta V_2^{sup} - \Delta V_j^p \right) \tag{18}$$

In (11)–(18), ΔV_{1_k} and ΔV_{2_k} are intermediary signals of the PSS dynamic model, while $\Delta Y_1, \Delta Y_2$, and ΔY_3 are intermediary signals of the POD dynamic model. More information about (11)–(18) can be found in [3,29]. Additionally, it is customary to adopt $T_1^{pss} = T_3^{pss}$ and $T_2^{pss} = T_4^{pss}$ for the PSS, and $T_1^{pod} = T_3^{pod}$ and $T_2^{pod} = T_4^{pod}$ for the POD [1].

4. Technique for the design of the PSS and POD controllers

This section presents the VNS algorithm proposed for the design of the parameters of PSS and POD controllers. The multi-start algorithm, used in the tests for comparison, is also discussed.

4.1. VNS algorithm

Existing exact methods for nonlinear optimization are only able to perform well when several requirements are satisfied in the problem, such as the continuity of the objective function and the constraints, the existence of the first and second derivatives of the objective function and constraints, and the convexity of the feasible region [30]. The problem addressed in this work, besides presenting nonlinear algebraic equations in the formulation, has differential equations that make it impossible to derive a complete exact mathematical model of optimization to be solved using these exact methods. For this reason, a modern heuristic approach for solving the presented problem is proposed in this section.

A local search strategy for nonlinear optimization is able to find a local optimum of a problem that presents many different good quality solutions, i.e., multi-modal problems. When exact optimization methods are applied directly to solve this type of problem, it is probable that only local optimal solutions, strongly dependent on the initial point, will be found. To overcome this limitation, Hansen and Mladenović presented in [25] a simple and efficient metaheuristic, called variable neighborhood search (Algorithm 1), which can be obtained by extending a local search algorithm to perform systematic changes of neighborhoods, for

solving complex problems. Contrary to most local search techniques, the VNS algorithm does not follow a trajectory, but explores more distant neighborhoods of the current best solution.

According to Algorithm 1, initially, a sequence of neighborhoods $\mathcal{N}_k, k = 1, \ldots, k_{max}$ is defined. Since the problem in this work presents continuous variables, the neighborhoods are defined depending on the distance of a point $\mathbf{x}'$ from the current solution $\mathbf{x}$. Thus, if a point $\mathbf{x}'$ belongs to the hyperrectangle with center at $\mathbf{x}$, in which each edge i has length $\varphi_k(\bar{x}_i - \underline{x}_i)$, where $\underline{x}_i$ and $\bar{x}_i$ are the lower and upper bounds of variable i, respectively, and $0 < \varphi_k \leqslant 1$, $\varphi_1 < \varphi_2 < \cdots < \varphi_{k_{max}}$, then $\mathbf{x}' \in \mathcal{N}_k(\mathbf{x})$.

An initial solution $\mathbf{x}$, is then generated and its quality is evaluated using the objective function $F(\mathbf{x})$ presented in next section. In this work, this solution is randomly generated within the variables' bounds. The iterative process begins with $k \leftarrow 1$, and a solution $\mathbf{x}'$ is randomly generated in the neighborhood $\mathcal{N}_1(\mathbf{x})$.

Algorithm 1. Variable Neighborhood Search

---

1. **Initialization**. Select the set of neighborhood structures $\mathcal{N}_k, k = 1, \ldots, k_{max}$, that will be used in the search; find an initial solution $\mathbf{x}$; choose a stopping condition;
2. **Repeat** the following until the stopping condition is met:
   (a) Set $k \leftarrow 1$;
   (b) Until $k = k_{max}$, repeat the following steps:
     i. Generate a point $\mathbf{x}'$ at random from the kth neighborhood of $\mathbf{x}$ ($\mathbf{x}' \in \mathcal{N}_k(\mathbf{x})$);
     ii. Apply some local search method with $\mathbf{x}'$ as initial solution; denote with $\mathbf{x}''$ the local optimum obtained;
     iii. If this local optimum is better than the best solution found in the process, move there ($\mathbf{x} \leftarrow \mathbf{x}''$), and continue the search with $\mathcal{N}_1(k \leftarrow 1)$; otherwise, set $k \leftarrow k + 1$, if $k > k_{max}$, set $k \leftarrow 1$.

In the next step, a local search is applied with $\mathbf{x}'$ as an initial solution. The local search used is presented in the next subsection. The solution of the local search is denoted $\mathbf{x}''$.

Three situations may occur:

- $\mathbf{x}'' = \mathbf{x}$, i.e., $\mathbf{x}$ is the optimal solution of the neighborhood. In this case, $k \leftarrow k + 1$, and the algorithm continues in the next neighborhood;
- $\mathbf{x}'' \neq \mathbf{x}$ and $F(\mathbf{x}'') \geqslant F(\mathbf{x})$. In this case, a new local optimal was obtained, but with worse quality than the current solution. The algorithm continues in the next neighborhood ($k \leftarrow k + 1$);
- $\mathbf{x}'' \neq \mathbf{x}$ and $F(\mathbf{x}'') < F(\mathbf{x})$. A new solution, better than the current solution, was found. The current solution is updated ($\mathbf{x} \leftarrow \mathbf{x}''$), and the search restarts in the first neighborhood ($k \leftarrow 1$) of $\mathbf{x}$.

If the last neighborhood is reached ($k > k_{max}$) and no improvement is obtained, then the search restarts in the first neighborhood $k \leftarrow 1$.

4.2. Local search algorithm

The local search step of the VNS algorithm is performed using the cyclic coordinate method [30] (Algorithm 2). This method can be directly used to optimize a nondifferentiable nonlinear function. A line search is repeatedly performed in the directions $\mathbf{d}_1, \ldots, \mathbf{d}_n$, where $\mathbf{d}_i$ is a vector in which element i is a "1" and all the remaining elements are zeros, from an initial point $\mathbf{x}_1$. The order of the directions, in this paper, is generated randomly.

However, in order to perform a local search, only a fraction of the interval $\underline{x}_i$ and $\bar{x}_i$ of each variable is used, around the current solution of the VNS algorithm. The interval considered for each variable represented twenty percent of the total amplitude in each direction from the current solution $\mathbf{x}$, i.e., $x_i - \rho(\bar{x}_i - \underline{x}_i) \leqslant x_i \leqslant x_i - \rho(\bar{x}_i - \underline{x}_i), \rho = 0.2$. If a variable violates a limit $\underline{x}_i$ or $\bar{x}_i$, the value is fixed at the violated limit.

On the other hand, in order to validate this proposal, the cyclic coordinate method is applied directly to the problem in the multistart algorithm, considering the complete intervals for each variable.

Algorithm 2. Cyclic Coordinate Method

---

1. **Initialization**. Choose a scalar $\epsilon > 0$ to be used for terminating the algorithm, and let $\mathbf{d}_1, \ldots, \mathbf{d}_n$ be the coordinated directions. Choose an initial point $\mathbf{x}_1$, let $\mathbf{y}_1 \leftarrow \mathbf{x}_1$, let $k \leftarrow 1$ and $j \leftarrow 1$, and go to the **Main Step**;
2. **Main Step**.
   (a) Let γ_j be an optimal solution to the problem to minimize $F(\mathbf{y}_j + \gamma \mathbf{d}_j)$ subject to $\gamma \in [a_1, b_1]$ and let $\mathbf{y}_{j+1} \leftarrow \mathbf{y}_j + \gamma_j \mathbf{d}_j$. If $j < n$, replace j by $j + 1$, and repeat Step (a). Otherwise, if $j = n$, got to Step (b);
   (b) Let $\mathbf{x}_{k+1} \leftarrow \mathbf{y}_{k+1}$. If $||\mathbf{x}_{k+1} - \mathbf{x}_k|| < \epsilon$, then stop. Otherwise, let $\mathbf{y}_1 \leftarrow \mathbf{x}_{k+1}$, let $j \leftarrow 1$, and $k \leftarrow k + 1$, and go to Step (a).

The Fibonacci line search method [30] (Algorithm 3), which is a derivative-free algorithm, was chosen to minimize F in a given direction $\mathbf{d}_i$. This method minimizes a strictly quasiconvex function in a bounded interval $[a_1, b_1]$. The Fibonacci sequence $\{\mathcal{F}_k\}$, defined as $\mathcal{F}_{k+1} \leftarrow \mathcal{F}_k + \mathcal{F}_{k-1}, k = 1, 2, \ldots$, with $\mathcal{F}_0 = \mathcal{F}_1 = 1$, is used for reducing the interval of uncertainty.

Algorithm 3. Fibonacci Line Search Method

---

1. **Initialization**. Define a suitable final length of uncertainty $l > 0$ and a constant $\epsilon > 0$. Consider $[a_1, b_1]$ as the initial interval of uncertainty, and choose the number of calculations n such that $\mathcal{F}_n > (b_1 - a_1)/l$;
   Let $\gamma_1 \leftarrow a_1 + (\mathcal{F}_{n-2}/\mathcal{F}_n)(b_1 - a_1)$ and $\mu_1 \leftarrow a_1 + (\mathcal{F}_{n-1}/\mathcal{F}_n)(b_1 - a_1)$. Evaluate $F(\mathbf{y}_j + \gamma_1 \mathbf{d}_j)$ and $F(\mathbf{y}_j + \mu_1 \mathbf{d}_j)$,
   let $k \leftarrow 1$, and go to the **Main Step**;
2. **Main Step**.
   (a) If $F(\mathbf{y}_j + \gamma_k \mathbf{d}_j) > F(\mathbf{y}_j + \mu_k \mathbf{d}_j)$, go to Step (b); and if $F(\mathbf{y}_j + \gamma_k \mathbf{d}_j) \leqslant F(\mathbf{y}_j + \mu_k \mathbf{d}_j)$, go to Step (c);
   (b) Let $a_{k+1} \leftarrow \gamma_k$ and $b_{k+1} \leftarrow b_k$. Furthermore, let $\gamma_{k+1} \leftarrow \mu_k$, and let $\mu_{k+1} \leftarrow a_{k+1} + (\mathcal{F}_{n-k-1}/\mathcal{F}_{n-k})(b_{k+1} - a_{k+1})$. If $k = n - 2$, go to Step (e); otherwise, evaluate $F(\mathbf{y}_j + \mu_{k+1} \mathbf{d}_j)$ and go to Step (d);
   (c) Let $a_{k+1} \leftarrow a_k$ and $b_{k+1} \leftarrow \mu_k$. Furthermore, let $\mu_{k+1} \leftarrow \gamma_k$, and let $\gamma_{k+1} \leftarrow a_{k+1} + (\mathcal{F}_{n-k-2}/\mathcal{F}_{n-k})(b_{k+1} - a_{k+1})$. If $k = n - 2$, go to Step (e); otherwise, evaluate $F(\mathbf{y}_j + \gamma_{k+1} \mathbf{d}_j)$ and go to Step (d);
   (d) Set $k \leftarrow k + 1$ and go to Step (a);
   (e) Let $\gamma_n \leftarrow \gamma_{n-1}$ and $\mu_n \leftarrow \gamma_{n-1} + \epsilon$. If $F(\mathbf{y}_j + \gamma_n \mathbf{d}_j) > F(\mathbf{y}_j + \mu_n \mathbf{d}_j)$, let $a_n \leftarrow \gamma_n$ and $b_n \leftarrow b_{n-1}$. Otherwise, if $F(\mathbf{y}_j + \gamma_n \mathbf{d}_j) \leqslant F(\mathbf{y}_j + \mu_n \mathbf{d}_j)$, let $a_n \leftarrow a_{n-1}$ and $b_n \leftarrow \gamma_n$. Stop; the optimal solution is in the interval $[a_n, b_n]$.

4.3. Multi-start method

The multi-start algorithm (Algorithm 4) is an optimization method based on a strategy for restarting a search strategy from many different solutions. Basically, the technique presented in this paper consists of two steps: generating a random solution and performing an improvement step. These two steps must be repeated until the stop criterion is satisfied. The search strategy used is the same one used in the VNS algorithm (considering, in this case, the complete intervals for each variable). The efficiency of the multi-start algorithm will be compared to the VNS algorithm, in order to evaluate the performance of the latter.

Algorithm 4. Multi-Start Algorithm

---

1. **Initialization**. Set $k \leftarrow 1$;
2. **Main Step.** Until $k = k_{max}$, repeat the following steps:
   (a) **Generation**. Construct solution $\mathbf{x}_k$;
   (b) **Search**. Apply a search method to improve $\mathbf{x}_k$; Let $\mathbf{x}'_k$ be the solution obtained;
   (c) **Update**. If $\mathbf{x}'_k$ improves the best solution, update it; set $k \leftarrow k + 1$.

---

5. Evaluation function and bounds for the optimization procedure

Consider that $\mathbf{x}$ is a solution proposal obtained in the algorithms of the previous section. Its evaluation function, $F(\mathbf{x})$, is defined as shown in (19).

$$F(\mathbf{x}) = \sum_{i=1}^{n} \max\{\underline{\xi}_i - \xi_i, 0\} \tag{19}$$

In (19), n is the number of eigenvalues of interest in the problem, ξ_i is the damping of eigenvalue i in solution $\mathbf{x}$, and $\underline{\xi}_i$ is the minimum desired damping for eigenvalue i, defined by the system operator. Note that each $\underline{\xi}_i$ is determined in the CSM.

The proposed evaluation function will assume a value of zero when each eigenvalue of interest i presents a damping greater than $\underline{\xi}_i$. Because it is a continuous optimization problem, it is assumed that convergence is achieved when $F(\mathbf{x}) < \epsilon$, where $\epsilon = 0.005$.

A solution proposal is illustrated in Fig. 4, which contains the control variables of the problem, in this case, the time constants and gains of the supplementary damping controllers, PSS and IPFC–POD.

In Fig. 4, it is considered the representation of a solution proposal for an electric power system equipped with n PSSs and one IPFC–POD set, and $T_{1_l}^{pss}, T_{2_l}^{pss}, K_l^{pss}$ and $T_1^{pod}, T_2^{pod}, K^{pod}$ are the time constants and gains of the PSS controllers and IPFC–POD set, respectively.

In all the simulations performed, it was considered that the time constants of the washout blocks of both controllers and the inherent delay of the control device are fixed: $T_{\omega}^{pss} = 10$ seconds for the PSS (Fig. 3(a)), $T_{\omega}^{pod} = 1$ second and $T_m^{ipfc} = 0.005$ seconds (Fig. 3(b)) for the IPFC–POD set. In addition, the values of the coupling reactances of the transformers are equal to 0.01 p.u. (x_{in}, $n = j, k$).

Each variable of a solution proposal is bounded by its respective limits, as indicated in Table 1.

Next section presents the results obtained with the proposed method.

6. Tests and results

Three systems were used in the simulations: the Two-Area Symmetrical system [1], the New England system [3], and the Reduced Southern Brazilian system. The first objective was to test and validate the VNS algorithm proposed in this paper. The second objective was to show that PSS controllers perform damping local oscillation modes, while the IPFC–POD inserts damping to the inter-area modes.

6.1. Characteristics of the test systems

The Two-Area Symmetrical system, shown in Fig. 5(a), has 2 areas, 4 generators, 17 branches, and 12 buses, including two new buses (FB_1^k and FB_2^k) and two new transmission lines ($7-FB_1^k$ and $7-FB_2^k$), added in order to perform simulations with the IPFC. It was considered that this system was equipped with two PSSs, at generators G2 and G3, and an IPFC–POD (see Fig. 5(a)).

The New England system consists of 10 generators, 41 buses, and 48 transmission lines and its line diagram is shown in Fig. 5 (c). In this diagram, two fictitious buses, FB_1^n and FB_2^n, and two lines, $37-FB_1^n$ and $37-FB_2^n$, were included to perform simulations with the IPFC. This system was equipped with eight PSSs, at generators G1, G2, G3, G4, G5, G7, G8, and G9, and an IPFC–POD (see Fig. 5(c)).

Fig. 6 shows the Reduced Southern Brazilian system. This is a real system that comprises 10 generators, 45 buses, and 73 transmission lines. It was equipped with nine PSSs at generators G1, G2, G3, G4, G6, G7, G8, G9, and G10 (see Fig. 6). The locations of the PSSs in all systems were determined by the participation factors [1], which indicated the generators that were more involved in the formation of each local mode.

6.2. Static analysis

The case in which the IPFC was installed in the system, but did not perform the control of active and reactive power flows, will be referred to as Case A. The other case, when the IPFC was actuating, will be referred to as Case B. Table 2 shows the values of the variables that were used to represent the IPFC's series converters in the systems in which they were installed.

In Case A, shown in Table 2, it can be seen that the values of the variables that were used to represent the series converters of the IPFC device are zero, which indicates that the IPFC was included in the system, but it was not performing any control.
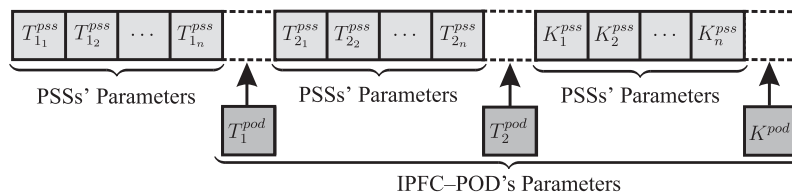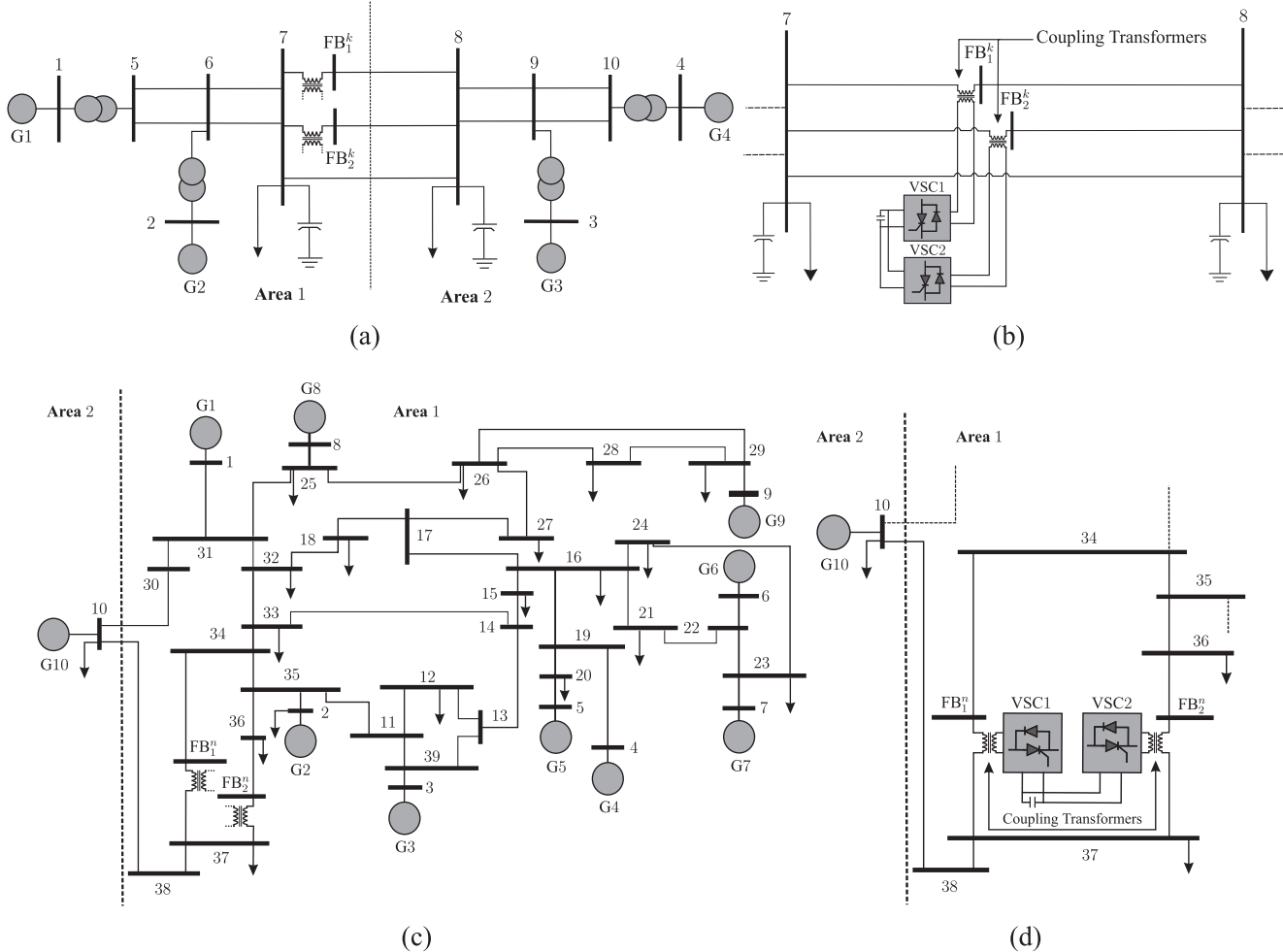

Fig. 4. Representation of a solution proposal.

Table 1
Bounds of the variables.

System	Limits	$T_{1_l}^{pss}$ [s]	$T_{2_l}^{pss}$ [s]	K_l^{pss} [p.u.]	T_1^{pod} [s]	T_2^{pod} [s]	K^{pod} [p.u.]
Two-Area Symmetrical	Min.	0.05	0.05	1.00	0.05	0.05	0.05
	Max.	1.00	1.00	5.00	1.00	1.00	1.50
New England	Min.	0.10	0.01	1.00	0.10	0.10	0.10
	Max.	1.50	0.10	10.00	0.40	0.40	0.50
Reduced Southern Brazilian	Min.	0.01	0.01	1.00	–	–	–
	Max.	0.50	0.25	12.00	–	–	–

Fig. 5. (a) One-line diagram of the Two-Area Symmetrical system, (b) insertion site of the IPFC in the Two-Area Symmetrical system, (c) one-line diagram of the New England system, and (d) insertion site of the IPFC in New England system.

In Figs. 5(b) and (d), it can be seen that the IPFC device was installed between buses 7 and 8 in the Two-Area Symmetrical system and between buses 34, 36, and 37 in the New England system. These locations were determined by technical factors. In the case of the Two-Area Symmetrical system, there are three transmission lines between buses 7 and 8. As the IPFC was installed in two lines to carry out the control of the flows, there was the possibility of having a slack line. Moreover, these are long lines, that are in parallel, with high inductive reactances, which favors the appearance of an inter-area oscillation mode. Finally, the voltage profile of the base case shown in Fig. 7(a) indicated that the voltage magnitude at bus 7 was lower than 0.95 p.u. (0.94 p.u.). It was expected that the IPFC device would improve the voltage profile at this bus, through the control of active and reactive power flows. In the New England system, the ideal place to install the IPFC device would be in the interconnection line between buses 10 and 38.

As there is only a line between these buses, it was impractical to install the device on this site; therefore, it was installed between buses 34, 36, and 37. The low voltage problems at buses 12, 15, 33, 36, and 37, lower than 0.95 p.u. (see Fig. 7(b)), also justified the installation of the IPFC at this location.

With the actuation of the IPFC device that controls active and reactive power flows on both the Two-Area Symmetrical system and the New England system, it can be verified that a new voltage profile was achieved for each one of these systems (Fig. 7(a) and (b)). In particular, the voltage magnitudes at bus 7 of the Two-Area Symmetrical system, and at buses 12, 15, 33, 36, and 37 of the New England system were improved, within the acceptable limits ($\pm 5\%$ of the nominal value).

For the results shown in Fig. 7(a) and (b), the flows on lines 7–FB_1^k and 7–FB_2^k of the Two-Area Symmetrical system were controlled (see Fig. 5(a) and (b)) by the IPFC device, with the following
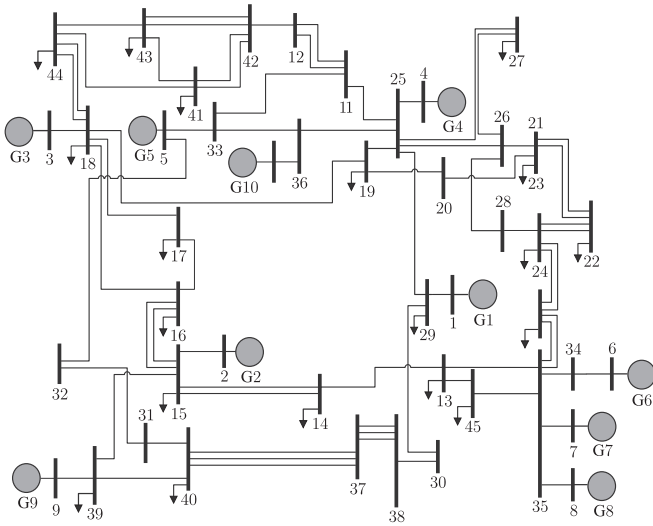
Fig. 6. One-line diagram of the Reduced Southern Brazilian system.

Fig. 7. Profiles of the voltage magnitudes of the (a) Two-Area Symmetrical system, (b) New England system, and (c) Reduced Southern Brazilian system.

values (Case B): $P_j^{ref} = 75.83$ MW (Case A: 64.81 MW), $Q_j^{ref} = -79.87$ MVAr (Case A: -24.96 MW), and $P_k^{ref} = 75.83$ MW (Case A: 64.81 MW). For the New England system, the flows on lines $FB_1^n - 34$ and $FB_2^n - 36$ (see Fig. 5(c) and (d)) were controlled, with the following values (Case B): $P_j^{ref} = -410.51$ MW (Case A: -310.98 MW), $Q_j^{ref} = -55.81$ MVAr (Case A: -42.28 MVAr), and $P_k^{ref} = -316.71$ MW (Case A: -241.76 MW).
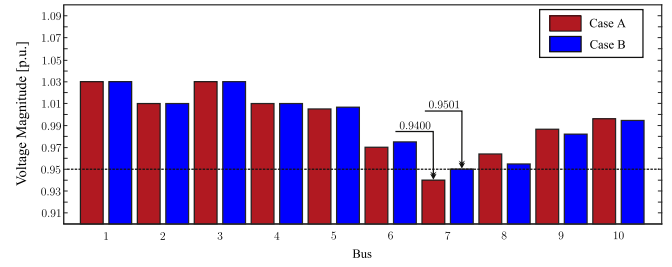
Figs. 8 and 9 show the active power flows in the Two-Area Symmetrical system and in the New England system (see Fig. 5) with and without the operation of the IPFC.

By analyzing the active power flows after the operation of the IPFC shown in Figs. 8 and 9, it is possible to verify that the device does not provide active power to the power system (active power invariance constraint of the IPFC), but it transfers, through the serial converters, active power for the lines on which the flows are controlled.
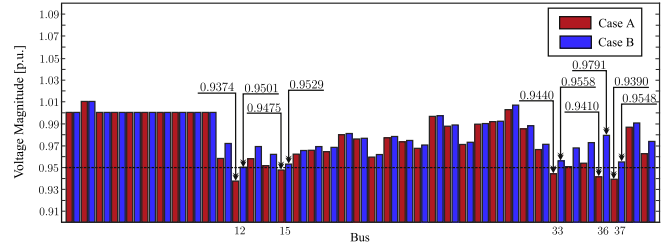
Regarding the Reduced Southern Brazilian system, there was no need to install an IPFC–POD device in this system. Two reasons justify this decision: first, as will be shown in Section 6.4, the system did not have any inter-area mode of oscillation and, thus, as will be proven, the PSS devices were enough to insert damping to the local mode electromechanical oscillations present in the electric power system; second, in Fig. 7(c), it can be seen that the voltage magnitudes at all buses were greater than 0.95 p.u. and, therefore, there was no need for an improvement of the voltage profile of this system.

6.3. Performance of the VNS algorithm

To evaluate the performance of the algorithms, the following was considered: (1) 100 tests limited to 2000 evaluations of the objective function; (2) the algorithms should be able to allocate all poles of interest with at least 10% of damping; (3) Repeat Case (2), considering at least 15% of damping for all modes of interest.

In the tests with the VNS and the multi-start algorithms, it was considered the evaluation function shown in (19). In all simulations (see Table 3), it was considered that the parameters of the controllers should satisfy the bounds shown in Table 1.

In Table 3, only the percentage of times that each algorithm has achieved convergence is shown. In addition, for the number of iterations (average, maximum, median, and standard deviation), only the tests in which the algorithms converged were considered.

For the Two-Area Symmetrical system, both algorithms had similar performance, converging for 100% of the tests. The difference between them, in this case, was related to the number of iterations necessary to achieve convergence. For both damping ranges ($\underline{\xi}_i = 10\%$ and $\underline{\xi}_i = 15\%$), on average and when the maximum number of iterations are compared, the VNS algorithm performance is better than the multi-start. The medians and the standard deviations also indicate better convergence rates for the VNS algorithm.

For the New England system, the VNS algorithm performed better for both damping ranges on the average, converging for the

Table 2
Variables of the IPFC's control structure.

IPFC	V_j^p [p.u.]	V_k^p [p.u.]	V_j^q [p.u.]	V_k^q [p.u.]
Two-Area Symmetrical System				
Case A	0.0000	0.0000	0.0000	0.0000
Case B	0.1187	0.0545	-0.2406	0.0964
New England System				
Case A	0.0000	0.0000	0.0000	0.0000
Case B	-0.2938	-0.3049	-0.0485	0.0048
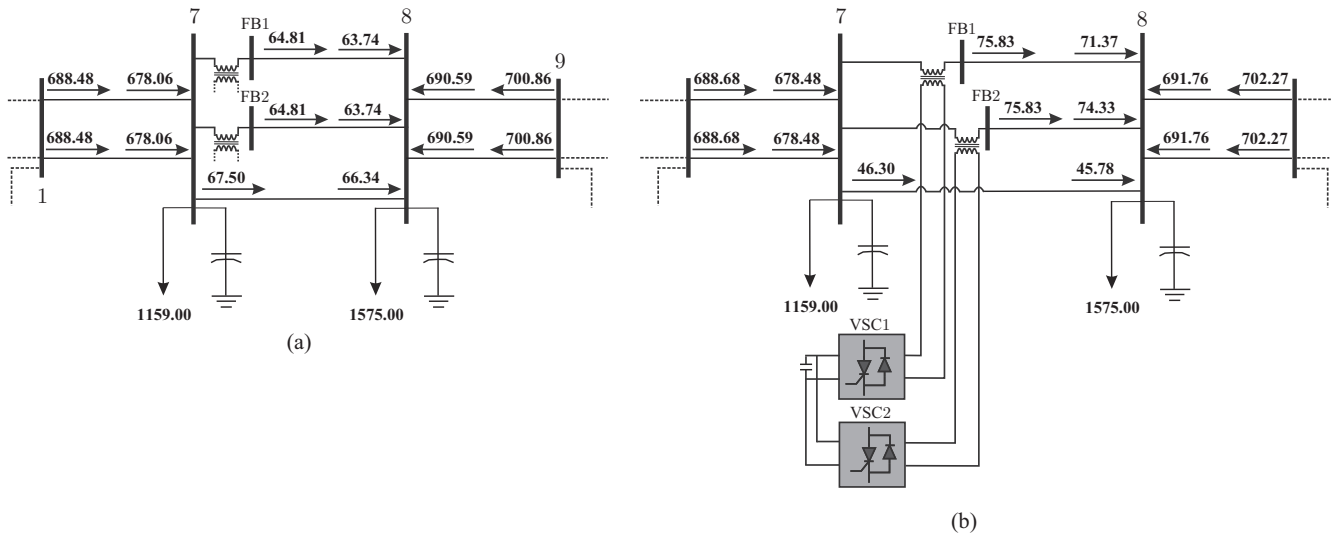
Fig. 8. Active power flow control performed by the IPFC in the Two-Area Symmetrical system. System (a) without the IPFC, and (b) with the IPFC.
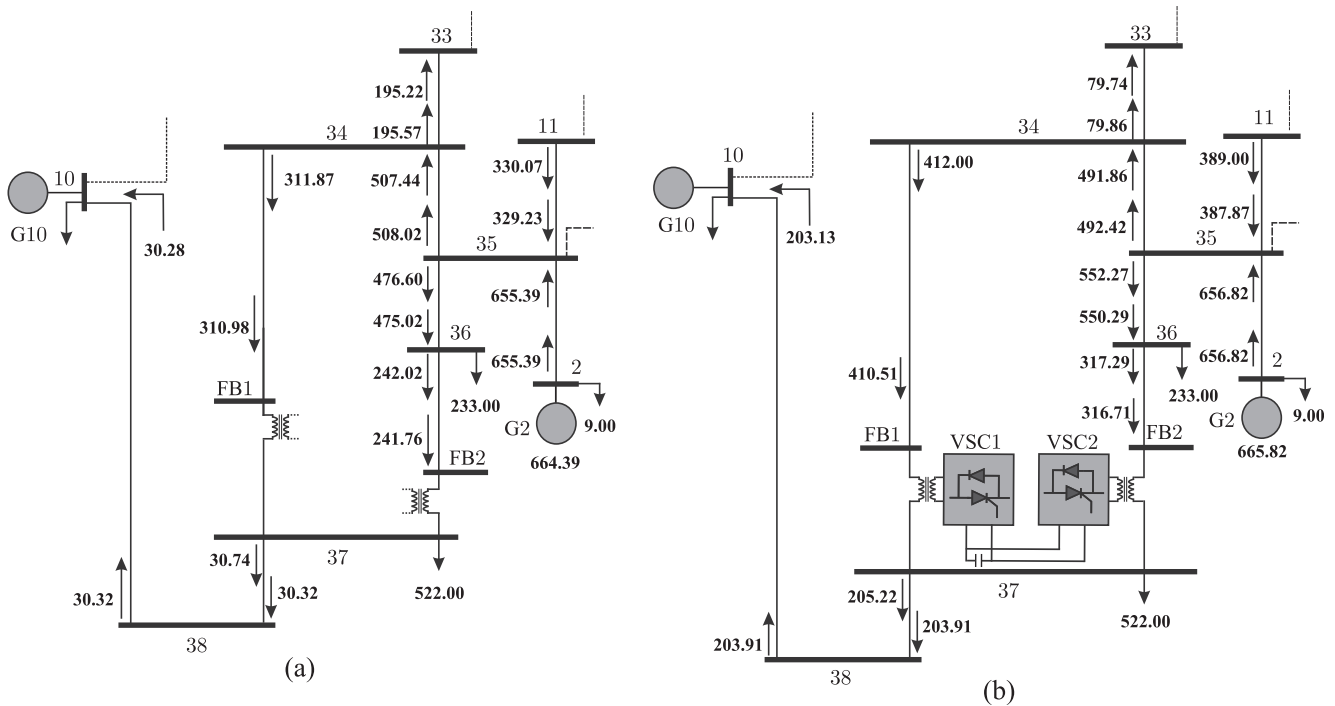
Fig. 9. Active power flow control performed by the IPFC in the New England system. System (a) without the IPFC, and (b) with the IPFC.

solution on 100% of the tests. For the second damping range, the multi-start algorithm converged for 96% of the tests.

Finally, for the Reduced Southern Brazilian system, for the first damping range ($\underline{\xi}_i = 10\%$), it can be observed that, on average, the VNS algorithm converged in one third of the iterations of the multi-start method. Also, for the damping range $\underline{\xi}_i = 15\%$, the VNS converged for 79% of the tests, while the multi-start converged for 50% of the tests.

Therefore, the statistical metrics presented in Table 3 indicate superior performance of the VNS metaheuristic when it is compared to the multi-start algorithm for optimizing the considered problem.

6.4. Dynamic analysis

This subsection presents the results for the dynamic analysis performed for the three systems considered.

In this paper, the parameters of the PI controllers of the dynamic model of the IPFC (see Fig. 2) were fixed, and they can be seen in Table 4.

6.4.1. Two-Area Symmetrical system

For this system, the tests are separated in Case A (without the actuation of the IPFC device to control the power flows, and not considering the POD and PSS controllers in the system) and Case B (with the actuation of the IPFC device). For Case B, three different scenarios were considered (besides the base case in which the PSS and POD controllers are not considered):

1. **Scenario I**: Considering only the installation of the IPFC–POD controller;
2. **Scenario II**: Considering only the installation of the two PSS controllers;

Table 3
Comparison the algorithms' performances.

Algorithm	$\underline{\xi}_i$ [%]	Converged tests [%]	Number of iterations			
			Average	Maximum	Median	Standard deviation
		Two-Area Symmetrical System				
VNS	10	100	43	65	41	9
	15	100	78	105	55	15
Multi-Start	10	100	52	140	49	28
	15	100	85	353	67	55
		New England System				
VNS	10	100	164	270	165	27
	15	100	449	1991	381	234
Multi-Start	10	100	294	1141	219	209
	15	96	607	1659	427	365
		Reduced Southern Brazilian System				
VNS	10	100	175	1465	89	95
	15	79	677	1902	382	307
Multi-Start	10	98	577	1905	497	441
	15	50	867	1978	767	532

Table 4
Parameters of the PI controllers of the dynamic model of the IPFC.

System	T_1^{pi} [s]	T_2^{pi} [s]	T_3^{pi} [s]	K_1^{pi} [p.u.]	K_2^{pi} [p.u.]	K_3^{pi} [p.u.]
Two-Area Symmetrical System	0.0872	0.0450	0.1000	3.3492	2.6010	1.2761
New England System	0.0074	0.0052	0.0056	0.8357	0.7555	0.9880

Table 5
Parameters of the PSS and IPFC–POD controllers adjusted by the VNS algorithm.

Scenario		Parameters	Device		
			PSS G1	PSS G2	IPFC–POD
I		T_1^{pod} [s]	–	–	1.0000
		T_2^{pod} [s]	–	–	0.4300
		K^{pod} [p.u.]	–	–	0.8100
II		T_1^{pss} [s]	1.0000	0.5250	–
		T_2^{pss} [s]	0.7150	0.2400	–
		K^{pss} [p.u.]	2.2000	1.4500	–
III	$\underline{\xi}_i = 10\%$	T_1^{pss}/T_1^{pod} [s]	0.7750	0.7600	0.9600
		T_2^{pss}/T_2^{pod} [s]	0.6400	0.5600	0.6400
		K^{pss}/K^{pod} [p.u.]	3.4000	3.8000	1.2000
	$\underline{\xi}_i = 15\%$	T_1^{pss}/T_1^{pod} [s]	1.0000	1.0000	0.9000
		T_2^{pss}/T_2^{pod} [s]	0.7000	0.6200	0.5200
		K^{pss}/K^{pod} [p.u.]	4.5000	4.6000	1.3000

3. **Scenario III**: Considering the installation of the two PSS and the IPFC–POD controller.

The purpose of these tests is to show that the PSS controllers have great impact on local oscillation modes, while the IPFC–POD has great influence in the inter-area mode. The minimum damping restriction of 10% ($\underline{\xi}_i = 10\%$) was used on the modes of interest for Scenarios I and II, and 10% and 15% ($\underline{\xi}_i = 15\%$) was imposed on the modes of interest for the tests in Scenario III.

The parameters of the controllers, obtained by the VNS algorithm, for the three scenarios are presented in Table 5. From the results obtained with the parameters for Scenarios I, II, and III,

Table 6
Damping ratios and natural undamped frequencies of the Two-Area Symmetrical system.

Mode	Case A		Case B									
			Base Case		Scenario I		Scenario II		Scenario III			
	ξ_i [p.u.]	ω_{n_i} [Hz]	ξ_i [p.u.]	ω_{n_i} [Hz]	ξ_i [p.u.]	ω_{n_i} [Hz]	ξ_i [p.u.]	ω_{n_i} [Hz]	ξ_i [p.u.]	ω_{n_i} [Hz]	ξ_i [p.u.]	ω_{n_i} [Hz]
λ_1	0.0544	1.0035	0.0578	1.0041	0.0548	1.0061	0.1065	1.0329	0.1091	1.0442	0.1510	1.0736
λ_2	0.0472	0.9409	0.0443	0.9419	0.0441	0.9427	0.1036	0.9435	0.1069	0.9813	0.1543	1.0102
λ_3	−0.0112	0.7063	−0.0118	0.7112	0.1004	0.5908	0.0019	0.7108	0.1018	0.6340	0.1506	0.6035

new dominant eigenvalues $(\lambda_i = \sigma_i \pm \omega_i)$, damping coefficients $\left(\xi_i = -\frac{\sigma_i}{|\lambda_i|}\right)$, and natural undamped frequencies $\left(\omega_{n_i} = \frac{|\lambda_i|}{2\pi}\right)$ were found for the Two-Area Symmetrical system. These results are presented in Table 6 along with the results for Case A and for the base case of Case B.

By analyzing the natural undamped frequencies of the eigenvalues shown in Table 6 for Case A, the existence of two local modes (λ_1 and λ_2) and an inter-area mode (λ_3) with positive real part can be verified, which characterizes the system as unstable.

Moreover, comparing the damping coefficients associated with the three oscillation modes before (Case A) and after (base case of Case B) the actuation of the IPFC device, a slight improvement of the damping associated with the local mode λ_1 can be verified. However, the device actuation negatively influenced the damping of the other two modes (λ_2 and λ_3).

For Case B, Scenario I, in the considered operating point, the test system was stable and the inter-area mode (λ_3) had more than 10% of damping. In this case, the damping of the local modes λ_1 and λ_2 remained almost unchanged, indicating that the IPFC–POD controller operated specifically in the inter-area oscillation mode. When Scenario II was considered, it was noticed that the joint

action of the PSS controllers, on generators G2 and G3, inserted damping (greater than 10%) to local modes. Although the system becomes stable, because the inter-area mode (λ_3) had negative real part, it was verified that the PSS controllers had a small influence in this oscillation mode. Under these conditions, small topological or parametric variations can lead to the system's instability. Finally, there was Scenario III, in which the joint action of the IPFC–POD and PSS controllers on generators G2 and G3 was effective. The system became stable, and all modes of interest of the system presented damping greater than 10% and 15% in the two sub-cases analyzed for Scenario III, i.e., the system presented a high margin of stability for the operating point considered.

6.4.2. Reduced Southern Brazilian system

The results for the base case presented in Table 7 indicates the presence of nine oscillation modes in the Reduced Southern Brazilian system. The presence of five modes with positive real part ($\lambda_1, \lambda_3, \lambda_4, \lambda_7,$ and λ_8) classified the system as unstable for the point of operation considered. Moreover, after the analysis of the natural undamped frequency of each mode of interest, each oscillation mode of the system can be classified as local.

Table 7
Damping ratios and natural undamped frequencies of the Reduced Southern Brazilian system.

Mode	Base Case		$\underline{\xi_i} = 10\%$		$\underline{\xi_i} = 15\%$	
	ξ_i [p.u.]	ω_{n_i} [Hz]	ξ_i [p.u.]	ω_{n_i} [Hz]	ξ_i [p.u.]	ω_{n_i} [Hz]
λ_1	−0.0144	1.1676	0.1025	1.2651	0.1819	0.9184
λ_2	0.0025	1.2531	0.1047	1.0072	0.2833	1.1419
λ_3	−0.0140	1.0276	0.1098	1.3174	0.1500	1.2618
λ_4	−0.0185	1.2961	0.1027	1.1350	0.1500	1.2221
λ_5	0.0295	1.5621	0.1456	1.4591	0.2914	1.6518
λ_6	0.0141	1.5511	0.1081	1.6180	0.1859	0.9653
λ_7	−0.0027	1.1465	0.1015	1.0925	0.2345	0.9535
λ_8	−0.0120	1.0936	0.1006	1.0546	0.1837	1.0478
λ_9	0.0060	1.3926	0.1163	1.4578	0.2187	1.7364

Table 8
Gains and time constants of the PSS controllers adjusted by the VNS algorithm: Reduced Southern Brazilian system.

Device	$\underline{\xi_i} = 10\%$			$\underline{\xi_i} = 15\%$		
	T_1^{pss} [s]	T_2^{pss} [s]	K^{pss} [p.u.]	T_1^{pss} [s]	T_2^{pss} [s]	K^{pss} [p.u.]
PSS G1	0.1500	0.0400	5.8000	0.3875	0.1156	3.5657
PSS G2	0.1100	0.1000	3.9000	0.1213	0.0611	11.0406
PSS G3	0.1240	0.0700	7.4400	0.4780	0.1878	3.1835
PSS G4	0.1100	0.0590	9.9200	0.2469	0.1615	10.9989
PSS G6	0.1000	0.0820	4.0150	0.1399	0.1243	8.0107
PSS G7	0.0680	0.0900	2.3000	0.2878	0.0760	6.3876
PSS G8	0.1550	0.0280	4.1400	0.1553	0.0539	5.1054
PSS G9	0.1100	0.0420	6.4000	0.2562	0.1590	7.9824
PSS G10	0.0850	0.0970	5.5000	0.2031	0.2179	11.8336

Table 9
Damping ratios and natural undamped frequencies of the New England system.

Mode	Case A		Case B					
			Base Case		$\underline{\xi_i} = 10\%$		$\underline{\xi_i} = 15\%$	
	ξ_i [p.u.]	ω_{n_i} [Hz]	ξ_i [p.u.]	ω_{n_i} [Hz]	ξ_i [p.u.]	ω_{n_i} [Hz]	ξ_i [p.u.]	ω_{n_i} [Hz]
λ_1	−0.0100	1.0918	−0.0070	1.0922	0.1134	1.0087	0.1528	1.1759
λ_2	0.0282	1.1609	0.0301	1.1637	0.1258	1.1212	0.1980	1.0427
λ_3	0.0235	1.3159	0.0243	1.3169	0.1421	1.0649	0.1540	1.0346
λ_4	−0.0251	0.9490	−0.0253	0.9489	0.1291	1.1525	0.1542	1.2779
λ_5	0.0184	1.0330	0.0184	1.0369	0.1006	1.1379	0.1659	1.2166
λ_6	0.0332	1.2901	0.0207	1.2914	0.1094	1.2544	0.1932	1.0449
λ_7	0.0292	1.3244	0.0289	1.3251	0.1004	0.9058	0.1681	0.9714
λ_8	−0.0226	1.0151	−0.0284	1.0170	0.1165	0.8118	0.1500	0.7600
λ_9	−0.0085	0.6152	−0.0075	0.6150	0.1110	0.6720	0.1683	0.6428

After processing the VNS algorithm, the parameters of the supplementary damping controllers were obtained (Table 8).

In Table 7, the adjustments made for the parameters of the PSS controllers by the VNS algorithm satisfied the two minimum damping restrictions for the local oscillation modes: $\underline{\xi}_i = 10\%$ and $\underline{\xi}_i = 15\%$. With the parameters shown in Table 8, new dominant eigenvalues, damping coefficients, and natural undamped frequencies were calculated for the system. Table 7 shows the two new operating states for the Reduced Southern Brazilian system, both with at least 10% and 15% of damping for the system's modes of interest (local modes).

The new operating states obtained for the Reduced Southern Brazilian system ($\underline{\xi}_i = 10\%$ and $\underline{\xi}_i = 15\%$), after the adjustments of the parameters of the PSS controllers, carried out by the VNS algorithm, indicated that the system was stable and operating with high levels of damping. The results obtained from the simulations performed with this test system allow us to confirm the conclusions of Section 6.4.1, i.e., PSS controllers are efficient to insert damping to local oscillation modes; therefore, there was no need

to install another supplementary damping controller in this system.

6.4.3. New England system

The tests for the New England system were separated in Case A (without the actuation of the IPFC device to control the power flows, and not considering the POD and PSS controllers in the system) and Case B (with the actuation of the IPFC device). The base case for Case B does not consider the PSS and POD controllers in the system. The results for this system are presented in Table 9.

Based on the analysis of Table 9, it can be concluded that the IPFC alone did not have good performance in damping the low-frequency oscillations present in the New England system (base case of Case B). Improvements are noted in the damping of the local modes λ_4, λ_6, λ_7, and λ_8. The negative influence in the damping can be verified on local modes λ_1, λ_2, and λ_3, and on the inter-area mode λ_9. Local mode λ_5 maintained the same damping before and after the inclusion and actuation of the IPFC device for the control of active and reactive power flows in the New England system.

Table 10
Gains and time constants of the PSS and IPFC–POD controllers adjusted by the VNS algorithm: New England system.

Device	$\underline{\xi}_i = 10\%$			$\underline{\xi}_i = 15\%$		
	T_1^{pss}/T_1^{pod} [s]	T_2^{pss}/T_2^{pod} [s]	K^{pss}/K^{pod} [p.u.]	T_1^{pss}/T_1^{pod} [s]	T_2^{pss}/T_2^{pod} [s]	K^{pss}/K^{pod} [p.u.]
PSS G1	1.4058	0.0289	6.6325	1.3250	0.0880	9.6218
PSS G2	0.5917	0.0387	5.0707	0.6200	0.0378	9.1768
PSS G3	0.6153	0.0474	6.0067	0.5291	0.0230	9.6135
PSS G4	0.5798	0.0165	6.2044	0.4907	0.0600	7.3980
PSS G6	0.4691	0.0571	6.2734	0.4839	0.0629	7.5139
PSS G7	0.3453	0.0391	4.8987	0.3971	0.0736	2.4905
PSS G8	0.5374	0.0414	4.6806	0.6408	0.0371	9.5487
PSS G9	0.3946	0.0583	1.8491	0.2792	0.0829	7.8125
IPFC–POD	0.1138	0.1788	0.3088	0.1142	0.3848	0.4832
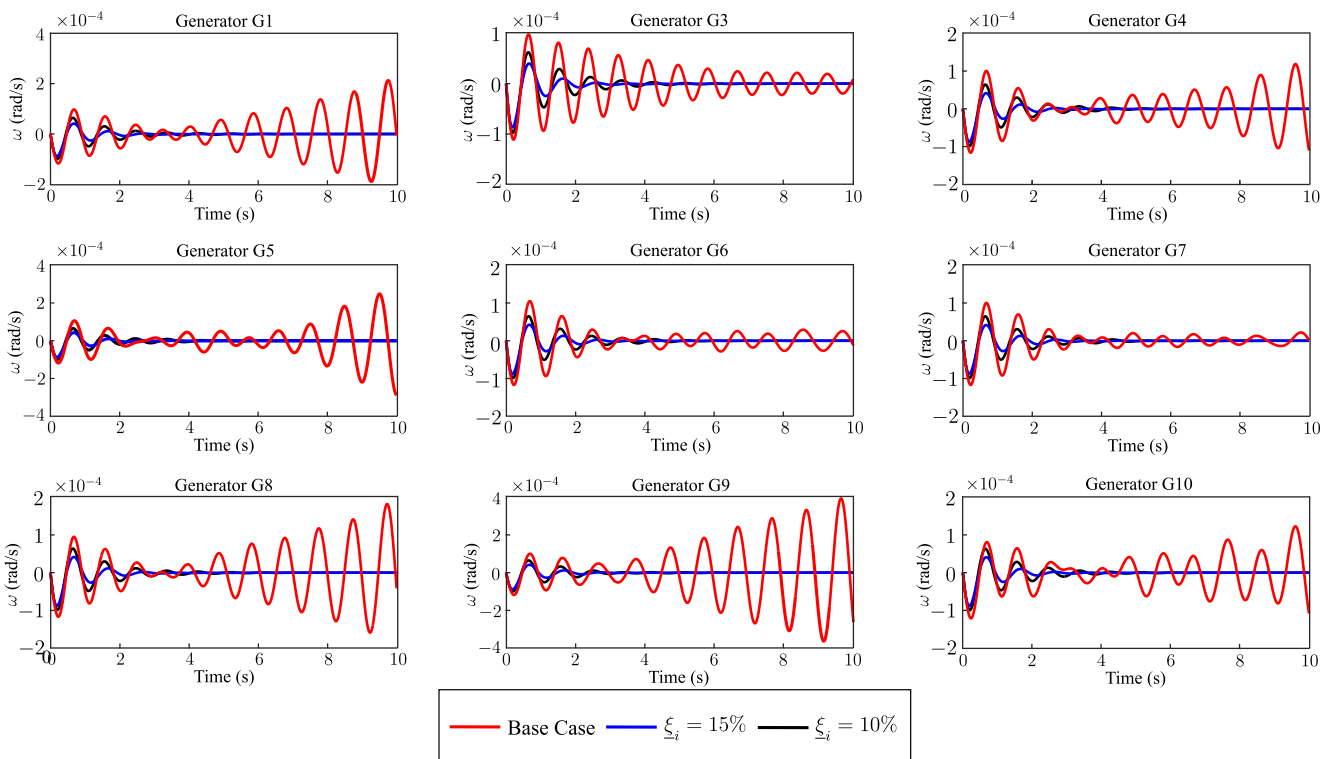
Fig. 10. Variations of the angular velocity of generators G1, G3, G5, G6, G7, G8, G9, and G10 in the New England system.

The New England system was characterized by having eight local oscillation modes and one inter-area mode. Thus, according to Sections 6.4.1 and 6.4.2, eight PSS and an IPFC–POD controllers were added in this system to insert damping to local and inter-area modes, respectively.

In Table 10, the results obtained by the VNS algorithm for the parameters of the PSS and IPFC–POD controllers to a valid state are shown, i.e., they satisfy (19) and the bounds shown in Table 1, which made it possible to modify the damping levels for the base case of Case B shown in Table 9 to values greater than or equal to 10% ($\underline{\xi}_i = 10\%$) and 15% ($\underline{\xi}_i = 15\%$) for all oscillation modes, i.e., local and inter-area modes.

By setting the New England system with the parameters of the PSS and IPFC–POD controllers according to Table 10, new dominant eigenvalues, damping coefficients, and natural undamped frequencies were calculated, obtained through simulations and shown in Table 9 with two new operating states, both with at least 10% and 15% of damping for the modes of interest.

The new operating states obtained for the New England system presented in Table 9 ($\underline{\xi}_i = 10\%$ and $\underline{\xi}_i = 15\%$) show a high damping margin for this test system and confirm that the joint action of the PSS and the IPFC–POD is able to insert damping to local and inter-area modes of oscillation when their control parameters are designed correctly.

Fig. 10 shows the variations of the angular velocities of generators G1, G3, G4, G5, G6, G7, G8, G9, and G10 of the New England system in relation to the variation of the angular velocity of gener-ator G2, the reference in the system, in which a step of 0.05 p.u. was applied to the mechanical power. In the cases presented in Fig. 10, the three scenarios already analyzed for Case B were con-sidered (see Table 9): Base Case, $\underline{\xi}_i = 10\%$, and $\underline{\xi}_i = 15\%$.

The electric power systems are subject to loading variations and consequent generation adjustments. The perturbations on the mechanical powers of the generators shown in Fig. 10 can be com-pared to these small generation adjustments. The curves in red represent the Base Case, while the black ($\underline{\xi}_i = 10\%$) and blue ($\underline{\xi}_i = 15\%$) curves represent the cases in which the system operates with high stability margin, equipped with eight PSS controllers and one IPFC–POD set, with parameters designed using the VNS algo-rithm. By analyzing Fig. 10, it can be verified that the curves repre-senting the Base Case, after the applied perturbation, are characterized by increasing or low damped amplitudes, typical of an unstable system (see Table 9). In the other two cases, even after the perturbation, the analysis of the obtained curves shows that the system is well damped, evidencing its high margin of stability to small-signal perturbations.

In order to verify the robustness of the parameters provided by the VNS algorithm, different loading scenarios are considered. The objective is to perform an analysis of the displacements of the oscillation modes of interest of the New England system (see Fig. 11). The loading scenarios are the following: $P\uparrow, Q\downarrow$: an increase of 5% on the active loads and a decrease of 5% on the reac-tive loads; $P\downarrow, Q\uparrow$: a decrease of 5% on the active loads and an increase 5% on the reactive loads; $P\downarrow, Q\downarrow$: a decrease of 5% on both active and reactive loads; $P\uparrow, Q\uparrow$: an increase of 5% on both active and reactive loads.

By analyzing Fig. 11, it can be verified that the damping levels in the New England system remained almost unchanged, even after the variations of the loads. In other words, the New England sys-tem was still able to operate with high damping levels for different load scenarios, evidencing the robustness of the parameters pro-vided by the VNS algorithm.
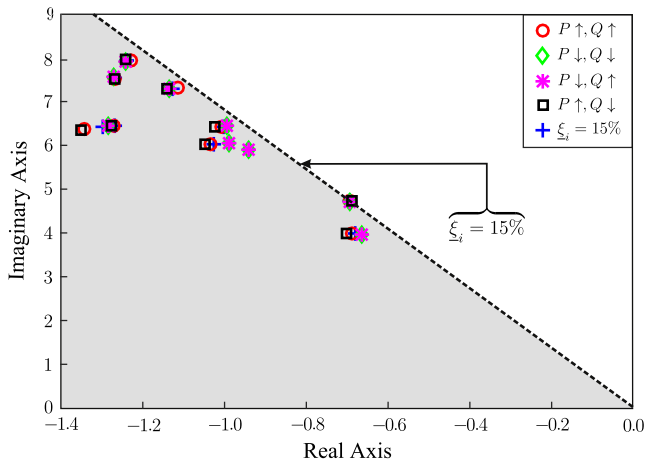
7. Conclusion

In this paper, a variable neighborhood search algorithm for the coordinated design of the parameters of supplementary damping controllers (power system stabilizers and interline power flow controller–power oscillation damping controller) was presented. The objective was to insert damping to small-signal local and inter-area oscillation modes present in the power system. The effectiveness of the technique was evaluated using the Two-Area Symmetrical, the New England, and the Reduced Southern Brazil-ian systems.

Fig. 11. Positioning of the eigenvalues of interest on the complex plane for the New England system.

Table 11
Synchronous generators and excitation system data for the Reduced Southern Brazilian system.

Generator (k)	Synchronous generators						Excitation system	
	x'_{d_k} [p.u.]	x_{d_k} [p.u.]	x_{q_k} [p.u.]	H_k [s]	D_k [p.u.]	$T'_{d_{0k}}$ [s]	K^r_k [p.u.]	T^r_k [s]
1	0.0457	0.1460	0.1050	37.32	0.10	6.90	200.00	0.001
2	0.0985	0.4015	0.2979	11.30	0.00	4.90	200.00	0.001
3	0.0300	0.0973	0.0700	39.46	0.00	8.27	200.00	0.001
4	0.0180	0.0561	0.0400	74.40	0.00	7.92	200.00	0.001
5	0.0215	0.0679	0.0500	57.28	0.00	10.00	200.00	0.001
6	0.1350	1.0150	0.7700	3.56	0.00	5.00	200.00	0.001
7	0.1535	0.9130	0.5304	5.06	0.00	4.89	200.00	0.001
8	0.1007	0.4000	0.2987	9.68	0.00	6.66	200.00	0.001
9	0.0550	0.2211	0.1235	20.34	0.00	9.55	200.00	0.001
10	0.0184	0.0730	0.0525	51.63	0.00	7.59	200.00	0.001

Table 12
Line and bus data for the Reduced Southern Brazilian system.

Initial bus (i)	End bus (j)	r_{ij} [p.u.]	x_{ij} [p.u.]	b_{ij}^{sh} [p.u.]	P_j^g [MW]	Q_j^g [MVAr]	P_j^l [MW]	Q_j^l [MVAr]
29	1	0.0000	0.0135	0.0000	650.00	4.92	0.00	0.00
15	2	0.0000	0.0460	0.0000	215.00	64.24	0.00	0.00
18	3	0.0000	0.0114	0.0000	895.00	102.90	0.00	0.00
25	4	0.0000	0.0067	0.0000	1531.60	−39.49	0.00	0.00
33	5	0.0000	0.0114	0.0000	1325.00	−4.78	0.00	0.00
34	6	0.0000	0.0871	0.0000	90.00	41.09	0.00	0.00
35	7	0.0000	0.0701	0.0000	120.00	45.51	0.00	0.00
35	8	0.0000	0.0450	0.0000	241.00	75.96	0.00	0.00
39	9	0.0000	0.0236	0.0000	460.00	98.12	0.00	0.00
36	10	0.0000	0.0068	0.0000	1100.00	−80.83	0.00	0.00
12	11	0.0007	0.0145	1.5672	0.00	0.00	0.00	0.00
11	12	0.0007	0.0145	1.5672	0.00	0.00	0.00	0.00
14	13	0.0386	0.1985	0.3425	0.00	0.00	177.00	68.00
15	14	0.0463	0.3378	0.3917	0.00	0.00	191.00	42.00
14	15	0.0463	0.3378	0.3917	0.00	0.00	171.00	18.50
15	16	0.0163	0.0835	0.1411	0.00	0.00	126.00	47.00
16	17	0.0163	0.0835	0.1445	0.00	0.00	46.00	14.70
16	18	0.0316	0.1621	0.2746	0.00	0.00	281.00	56.50
18	19	0.0306	0.1523	0.2620	0.00	0.00	279.00	60.70
19	20	0.0245	0.1256	0.1981	0.00	0.00	130.00	29.40
20	21	0.0088	0.0415	0.5009	0.00	0.00	427.00	−25.00
23	22	0.0154	0.0776	0.1386	0.00	0.00	310.00	141.00
22	23	0.0154	0.0776	0.1386	0.00	0.00	424.00	90.60
23	24	0.0216	0.1105	0.1872	0.00	0.00	117.00	53.10
11	25	0.0018	0.0227	2.1230	0.00	0.00	0.00	0.00
25	26	0.0019	0.0280	3.1526	0.00	0.00	0.00	0.00
25	27	0.0019	0.0274	3.0741	0.00	0.00	368.00	59.60
23	28	0.0000	0.0062	0.0000	0.00	0.00	0.00	0.00
25	29	0.0014	0.0195	2.2505	0.00	0.00	174.00	−8.00
29	30	0.0021	0.0300	3.5289	0.00	0.00	0.00	0.00
40	31	0.0000	0.0062	0.0000	0.00	0.00	0.00	0.00
31	32	0.0022	0.0300	3.6137	0.00	0.00	0.00	0.00
11	33	0.0014	0.0204	2.2869	0.00	0.00	0.00	0.00
35	34	0.0000	0.0590	0.0000	0.00	0.00	125.00	39.80
24	35	0.0180	0.0920	0.1556	0.00	0.00	0.00	0.00
33	36	0.0005	0.0070	0.7856	0.00	0.00	0.00	0.00
38	37	0.0021	0.0107	0.0208	0.00	0.00	813.00	110.00
37	38	0.0021	0.0107	0.0208	0.00	0.00	612.00	−455.00
40	39	0.0202	0.1129	0.1993	0.00	0.00	404.00	135.00
37	40	0.0184	0.0949	0.0000	0.00	0.00	393.00	−111.00
42	41	0.0106	0.0596	0.0951	0.00	0.00	262.00	13.20
12	42	0.0000	0.0063	0.0000	0.00	0.00	229.00	183.00
41	43	0.0110	0.1184	0.2081	0.00	0.00	184.00	60.20
41	44	0.0229	0.1174	0.2087	0.00	0.00	139.00	53.70
35	45	0.0129	0.0657	0.1155	0.00	0.00	90.10	55.30
32	33	0.0014	0.0195	2.2441				
37	38	0.0021	0.0107	0.0208				
37	40	0.0184	0.0949	0.0000				
37	40	0.0184	0.0949	0.0000				
41	42	0.0106	0.0596	0.0951				
42	43	0.0172	0.0884	0.1446				
42	43	0.0172	0.0884	0.1446				
43	44	0.0181	0.0929	0.1671				
13	35	0.0096	0.0491	0.0861				
13	45	0.0033	0.0167	0.3019				
14	37	0.0177	0.0910	0.1510				
14	37	0.0177	0.0910	0.1510				
14	37	0.0177	0.0910	0.1510				
15	16	0.0163	0.0835	0.1411				
15	39	0.0250	0.1648	0.4581				
17	18	0.0153	0.0861	0.1328				
18	44	0.0344	0.1760	0.3061				
18	44	0.0344	0.1760	0.3061				
19	25	0.0000	0.0300	0.0000				
21	22	0.0182	0.0935	0.1602				
21	22	0.0182	0.0935	0.1602				
21	26	0.0000	0.0062	0.0000				
23	24	0.0216	0.1105	0.1872				
24	35	0.0180	0.0920	0.1556				
25	36	0.0005	0.0070	0.7857				
26	27	0.0005	0.0069	0.7728				
26	28	0.0012	0.0175	2.0160				
30	38	0.0000	0.0062	0.0000				

- The performance of the VNS algorithm was compared to a multi-start method. The results showed that the VNS algorithm was more efficient for solving the problem, accrediting it as a powerful tool for the design of controllers and for the analysis of small-signal stability in electric power systems.
- The results presented corroborate the fact that the supplementary damping controllers, with properly adjusted parameters, are able to insert damping to both local and inter-area oscillation modes.
- In particular, it was possible to conclude that the power system stabilizers are capable of inserting damping to the generators' low frequency oscillations, i.e., the local modes, increasing the margin of stability to small-signal disturbances. Moreover, it was shown that the interline power flow controller–power oscillation damping controller operates mainly by inserting damping to the inter-area oscillation modes.
- A robustness analysis demonstrated that the solutions obtained by the VNS algorithm provided high levels of damping even when the operating point of the system changed.

Future work in this subject can be related to including the robustness analysis into the metaheuristic framework to ensure a minimum damping level for a range of operating conditions. Also, advanced stabilizers, such as multi-band, can be considered. It is also possible to extend the formulation to a planning problem, with the objective to find the best places to install the controllers in the system.

Acknowledgment

Appendix A

Complete data for the Reduced Southern Brazilian system, used in the CSM [3], is provided in Tables 11 and 12. It is assumed that bus 4 is the reference bus. The apparent power base is 100 MVA and the voltage base is 345 kV.

References

[1] Kundur P. Power system stability and control. New York: MacGraw-Hill; 1994.
[2] Larsen E, Swann D. Applying power system stabilizers part II: performance objectives and tuning concepts. IEEE Trans Power Apparat Syst 1981;PAS-100(6):3025–33.
[3] Fortes EV, Araujo PB, Macedo LH. Coordinated tuning of the parameters of PI, PSS and POD controllers using a specialized Chu-Beasley's genetic algorithm. Electr Power Syst Res 2016;140:708–21.
[4] De Mello FP, Concordia C. Concepts of synchronous machine stability as affected by excitation control. IEEE Trans Power Apparat Syst 1969;88(4):316–29.
[5] Noroozian M, Andersson G. Damping of power system oscillations by use of controllable components. IEEE Trans Power Deliv 1994;9(4):2046–54.
[6] Valle DB, Araujo PB. The influence of GUPFC FACTS device on small signal stability of the electrical power systems. Int J Electr Power Energy Syst 2015;65:299–306.
[7] Gyugyi L, Sen K, Schauderr CD. The interline power flow controller concept: a new approach to power flow management in transmission systems. IEEE Trans Power Deliv 1999;14(3):1115–23.
[8] Yang N, Liu Q, McClley JD. TCSC controller design for damping interarea oscillations. IEEE Trans Power Syst 1998;13(14):1304–10.
[9] Chen CL, Hsu YY. Coordinated synthesis of multimachine power system stabilizer using an efficient decentralized modal control (DMC) algorithm. IEEE Trans Power Syst 1987;2(3):543–50. http://dx.doi.org/10.1109/TPWRS.1987.4335165.
[10] Araujo PB, Zaneta LC. Pole placement method using the system matrix transfer function and sparsity. Int J Electr Power Syst Energy Syst 2001;23(3):173–8.
[11] Abd-Elazim SM, Ali ES. Power system stability enhancement via bacteria foraging optimization algorithm. Arab J Sci Eng 2013;38(3):599–611.
[12] Abd-Elazim SM, Ali ES. Coordinated design of PSSs and SVC via bacteria foraging optimization algorithm in a multimachine power system. Int J Electr Power Energy Syst 2012;41(1):44–53.
[13] Mondal D, Chakrabarti A, Sengupta A. Optimal placement and parameter setting of SVC and TCSC using PSO to mitigate small signal stability problem. Int J Electr Power Energy Syst 2012;42(1):334–40.
[14] Hasanvand H, Arvan MR, Mozafari B, Amraee T. Coordinated design of PSS and TCSC to mitigate interarea oscillations. Int J Electr Power Energy Syst 2016;78:194–206.
[15] Shayeghi H, Safari A, Shayanfar HA. PSS and TCSC damping controller coordinated design using PSO in multi-machine power system. Energy Convers Manage 2010;51(12):2930–7.
[16] Hassan LH, Moghavvemi M, Almurib HAF, Muttaqi KM. A coordinated design of PSSs and UPFC-based stabilizer using genetic algorithm. IEEE Trans Ind Appl 2014;50(5):2957–66.
[17] Jolfaei MG, Sharaf AM, Shariatmadar SM, Poudeh MB. A hybrid PSS-SSSC GA-stabilization scheme for damping power system small signal oscillations. Int J Electr Power Energy Syst 2016;75:337–44.
[18] Bian XY, Geng Y, Lo KL, Fu Y, Zhou QB. Coordination of PSSs and SVC damping controller to improve probabilistic small-signal stability of power system with wind farm integration. IEEE Trans Power Syst 2016;31(3):2371–82.
[19] Gholipour E, Nosratabadi SM. A new coordination strategy of SSSC and PSS controllers in power system using SOA algorithm based on pareto method. Int J Electr Power Energy Syst 2015;67:462–71.
[20] Abd-Elazim SM, Ali ES. Optimal power system stabilizers design via cuckoo search algorithm. Int J Electr Power Energy Syst 2016;75:99–107.
[21] Fortes EV, Araujo PB, Macedo LH, Gamino BR, Martins LFB. Analysis of the influence of PSS and IPFC-POD controllers in small-signal stability using a simulated annealing algorithm. In: 2016 12th IEEE international conference on industry applications (INDUSCON); 2016. p. 1–8.
[22] Panda S, Yegireddy NK, Mohapatra SK. Hybrid BFOA-PSO approach for coordinated design of PSS and SSSC-based controller considering time delays. Int J Electr Power Energy Syst 2013;49:221–33.
[23] Abd-Elazim SM, Ali ES. Synergy of particle swarm optimization and bacterial foraging for TCSC damping controller design. WSEAS Trans Power Syst 2013;8(2):74–84.
[24] Khadanga RK, Satapathy JK. Time delay approach for PSS and SSSC based coordinated controller design using hybrid PSO-GSA algorithm. Int J Electr Power Energy Syst 2015;71:262–73.
[25] Hansen P, Mladenović N. Variable neighborhood search: principles and applications. Eur J Oper Res 2001;130(3):449–67.
[26] Glover F, Kochenberger G. Handbook of metaheuristics. Norwell MA, USA: Kluwer Academic; 2003.
[27] Zhang X-P. Modelling of the interline power flow controller and the generalised unified power flow controller in Newton power flow. IEE Proc–Gener, Transm Distrib 2003;150(3):268–74.
[28] Zhang J, Yokoyama A. Power system transient stability improvement by the interline power flow controller (IPFC). IEEJ Trans Power Energy 2008;128(1):208–15.
[29] Fortes EV. Application of the specialized Chu-Beasley's genetic algorithm for adjusting the parameters of supplementary controllers and the IPFC FACTS device [Ph.D. Thesis]. Ilha Solteira: School of Natural Sciences and Engineering, Sao Paulo State University; 2016. p. 73–77 [in Portuguese].
[30] Bazaraa MS, Sherali HD, Shetty CM. Nonlinear programming: theory and algorithms. 3rd ed. Wiley-Interscience; 2006.